The endothelial compartment as a disease modifier in bleeding disorders
Laan, S.N.J.

Citation
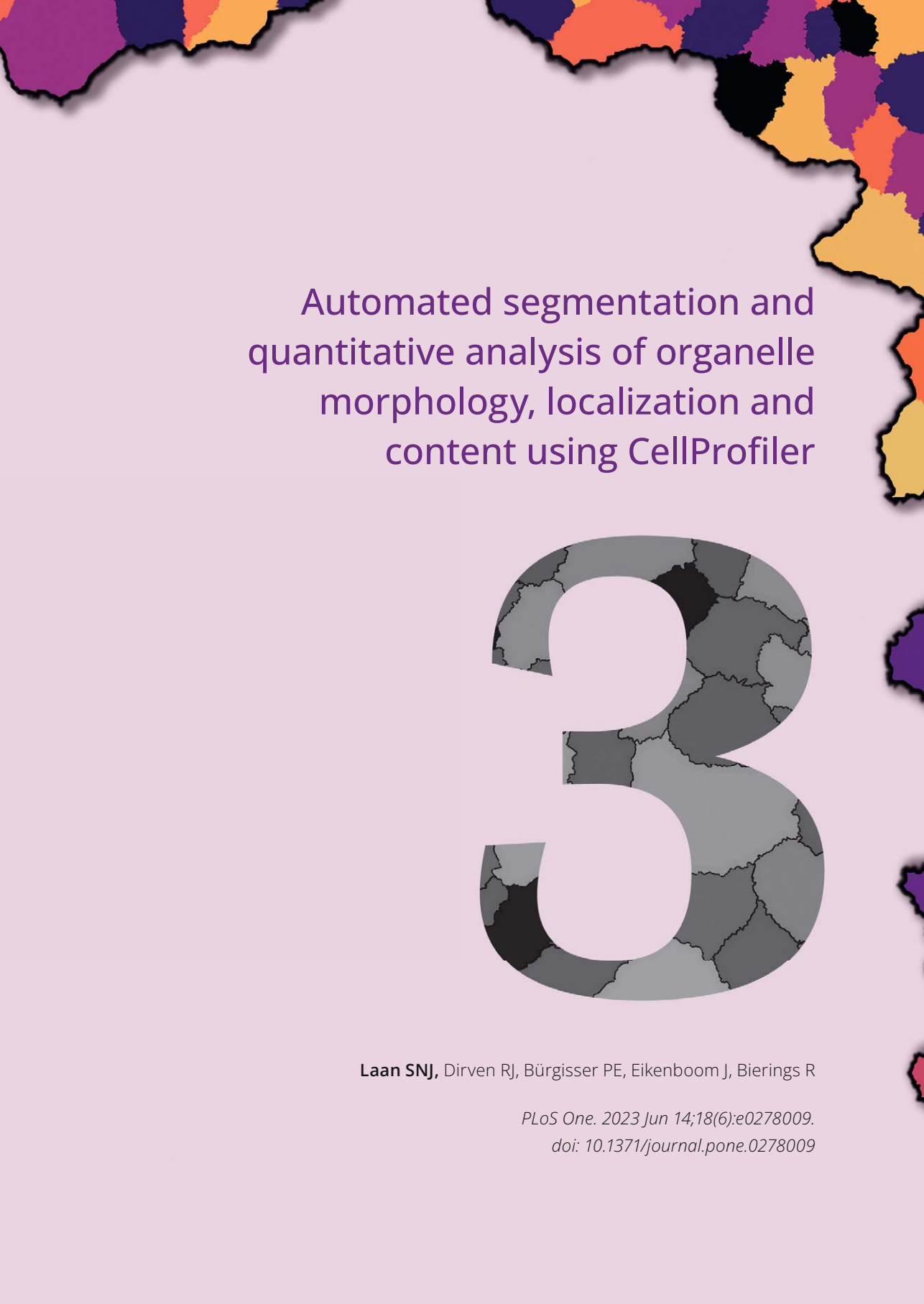Laan, S. N. J. (2025, September 24). *The endothelial compartment as a disease modifier in bleeding disorders*. Retrieved from https://hdl.handle.net/1887/4262075

|	
Version:	Publisher's Version
License:	Licence agreement concerning inclusion of doctoral thesis in the Institutional Repository of the University of Leiden
Downloaded from:	https://hdl.handle.net/1887/4262075

Note: To cite this publication please use the final published version (if applicable).

Automated segmentation and quantitative analysis of organelle morphology, localization and content using CellProfiler
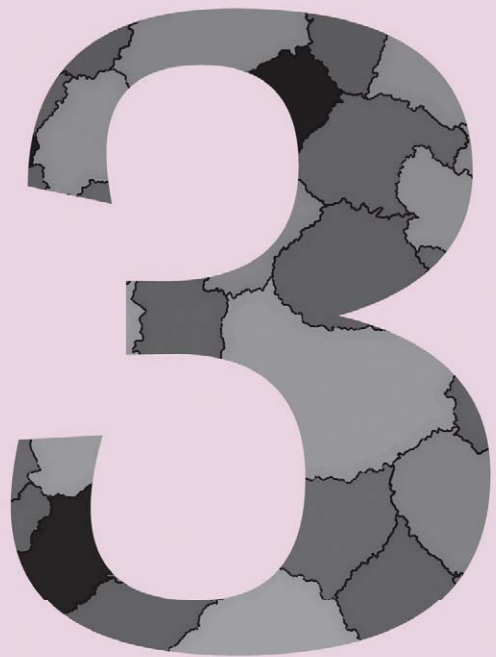
Laan SNJ, Dirven RJ, Bürgisser PE, Eikenboom J, Bierings R

Abstract

One of the most used and versatile methods to study number, dimensions, content and localization of secretory organelles is confocal microscopy analysis. However, considerable heterogeneity exists in the number, size and shape of secretory organelles that can be present in the cell. One thus needs to analyze large numbers of organelles for valid quantification. Properly evaluating these parameters requires an automated, unbiased method to process and quantitatively analyze microscopy data. Here, we describe two pipelines, run by CellProfiler software, called OrganelleProfiler and OrganelleContentProfiler. These pipelines were used on confocal images of endothelial colony forming cells (ECFCs), which contain unique secretory organelles called Weibel-Palade bodies (WPBs), and on early endosomes in ECFCs and human embryonic kidney 293T (HEK293T) cells. Results show that the pipelines can quantify the cell count, size, organelle count, organelle size, shape, relation to cells and nuclei, and distance to these objects in both endothelial and HEK293T cells. Additionally, the pipelines were used to measure the reduction in WPB size after disruption of the Golgi and to quantify the perinuclear clustering of WPBs after triggering of cAMP-mediated signaling pathways in ECFCs. Furthermore, the pipeline is able to quantify secondary signals located in or on the organelle or in the cytoplasm, such as the small WPB GTPase Rab27A. Cell profiler measurements were checked for validity using Fiji. To conclude, these pipelines provide a powerful, high-processing quantitative tool for the characterization of multiple cell and organelle types. These pipelines are freely available and easily editable for use on different cell types or organelles.

Introduction

Eukaryotic cells are compartmentalized into organelles, subcellular entities separated from the cytoplasm by a limiting membrane that enable them to more efficiently carry out specialized functions in the cell, such as energy production and protein synthesis, transport and degradation. A specific class of organelles consists of secretory vesicles, which serve to temporarily store and then rapidly secrete molecules into the extracellular space on demand. Secretory organelles are vital to maintaining homeostasis, as they allow a cell to communicate with other, distant cells or to respond to immediate changes in its environment, such as in the case of injury or when encountering pathogens. Their function is often defined by the content that is secreted, which is cell type and context specific, and depends on a sufficient magnitude of release, which directly relates to the number and dimensions of the secretory organelles that can undergo exocytosis. Moreover, the intracellular location of secretory organelles in relation to their site of biogenesis (i.e. the Golgi apparatus), filaments of the cytoskeleton and the plasma membrane also indirectly determines their exocytotic behavior.

Weibel-Palade bodies (WPBs) are cigar-shaped endothelial cell specific secretory organelles that contain a cocktail of vasoactive molecules that are released into the circulation in response to vascular injury or stress (1). WPBs owe their typical elongated morphology to the condensation of its main cargo protein, the hemostatic protein Von Willebrand factor (VWF), into organized parallel tubules that unfurl into long platelet-adhesive strings upon release (2). The size and shape of WPBs are of interest from a biological and medical perspective as they correlate with the hemostatic activity of the VWF strings that are released (3) and can be reflective of disease states, such as in the bleeding disorder von Willebrand disease (VWD) (4). A model frequently used to study the pathophysiology of vascular diseases like VWD is the endothelial colony forming cell (ECFC). A major advantage of this model is that ECFCs can be derived from whole blood of patients, which allows analysis of patient endothelial cell function, WPB morphology and secretion *ex vivo*. However, substantial phenotypic heterogeneity can exist between ECFCs (5, 6), which stresses the need for robust quantitative analytical methods to evaluate their phenotype.

One of the most used and versatile methods to study number, dimensions, content and localization of secretory organelles is confocal microscopy analysis. However, as with all biological samples, considerable variability exists in the number, size and shapes of secretory organelles that can be present in the cell. One thus needs to analyze large numbers of organelles while ideally collecting this information in such a manner that it can be analyzed in a cell-by-cell manner. The crowded intracellular environment

3

in combination with optical and immunostaining limitations presents an additional, technical challenge to separate individual organelles, which often precludes analysis on single organelle detail. Proper evaluation of these parameters requires an automated, unbiased method to process and quantitatively analyze microscopy data.

Here we describe 2 pipelines developed in CellProfiler (7), a free, easy to use image analysis software that uses separate module-based programming, for the identification, quantification and morphological analysis of secretory organelles within endothelial cells. The automated analysis pipeline OrganelleProfiler (OP) segments cells, organelles, nuclei and cell membranes from microscopy images, quantifies number, location, size and shape of organelles and extracts these data per cell and relative to the location of nucleus and perimeter of the cell. The function of the OrganelleProfiler pipeline is demonstrated by automated analysis of WPBs in 2 previously established phenotypic classes of healthy donor ECFCs (6), which identifies clear differences in number, length, eccentricity and intracellular localization of WPBs, and by morphometric analysis of early endosomes in ECFCs and HEK293T cells. Furthermore, the OrganelleProfiler was able to measure reduction in WPB size after Golgi ribbon disruption and to quantify perinuclear clustering of WPBs after stimulation with cAMP-mediated agonists. A second pipeline, called OrganelleContentProfiler (OCP), expands on the capabilities of the OrganelleProfiler by offering additional modules to measure the intensity of proteins of the secretory pathway both inside and outside the WPB, which we illustrate by analyzing the presence of the WPB GTPase Rab27A (8-10) and the endoplasmic reticulum marker protein disulfide isomerase (PDI).

Our CellProfiler pipelines provide robust and unbiased quantitative analysis tools for WPB morphometrics and can, with minimal adaptation, also be used to obtain quantitative data for other organelles and/or other cellular systems.

Materials & Methods

Endothelial Colony Forming Cells and Ethical Approval
The study protocols for acquisition of ECFCs were approved by the Leiden University Medical Center and Erasmus MC ethics review boards. Informed consent was obtained from 4 subjects in accordance with the Declaration of Helsinki. Healthy participants were 18 years or older and had not been diagnosed with or known to have VWD or any other bleeding disorder. ECFCs used in this study have previously been classified as group 1 or group 3 (6).

Cell Culture, Immunofluorescence and Image Acquisition

General cell culture of endothelial colony forming cells (ECFCs) and HEK293T cells was performed as described (5) and (11). ECFCs and HEK293T cells were grown on gelatin- or collagen-coated glass coverslips (9mm) and left confluent for 5 days before fixing with 70% methanol on ice for 10 minutes or with 4% paraformaldehyde for 15 minutes as described previously (10). Disruption of Golgi ribbons was done by exposure of ECFCs to 2 μg/ml of nocodazole (Sigma, M1404) for 46 hours. For triggering of cAMP-mediated signaling to induce perinuclear clustering of WPBs, post-confluent monolayers of ECFCs were treated with 10 μM Forskolin (Merck, F3917) and 100 μM 3-isobutyl-1-methylxanthine (IBMX) (Merck, I5879) for 30 minutes as described previously (12). Samples for OrganelleProfiler were stained with antibodies against VWF, EEA1, VE-cadherin, β-catenin, TGN46 and nuclei were stained with Hoechst or DAPI (Supplemental Table 1 for supporting information on antibodies). Samples for OrganelleContentProfiler were stained with Hoechst and antibodies against VWF, VE-cadherin and either Rab27A or PDI. After staining with appropriate fluorescently labeled secondary antibodies, coverslips were mounted using ProLong® Diamond Antifade Mountant (Thermo Fisher Scientific). Visualization of the cells for the OrganelleProfiler example was done using the Imagexpress Micro Confocal System using the 63x objective without magnification or with the Leica Stellaris 5 Low Incidence Angle using the 63x oil immersion objective. The OrganelleContentProfiler samples were imaged using the Zeiss LSM900 Airyscan2 upright confocal microscope using the 63x oil immersion objective. For both the OrganelleProfiler and OrganelleContentProfiler images a Z-stack was made which was transformed to a maximum Z-projection.

CellProfiler-Based pipelines for cell organelle analysis and manual scoring with Fiji

CellProfiler (version 4.2.1 at time of publication) was used, which can be downloaded from the CellProfiler website (www.cellprofiler.org). For the initial development of the pipelines, confocal images from 33 ECFC clones from several healthy donors were used. These ECFCs have previously been classified into separate phenotypic groups based on cellular morphology (6). The final pipeline was tested on 5 tile scans from one group 1 and one clone belonging to group 3. Images have to be of high enough resolution that individual organelles can be identified and do not blur together. Magnification, laser intensity, detector sensitivity and other acquisition parameters should be the same for each image set. Image format has to be similar as well. We recommend uncompressed TIFF files. Pipelines developed are available in the Supplementary Files (file 1 and 2) and have been deposited in our laboratory GitHUB repository (https://github.com/Clotterdam). Adjusted pipelines optimized for the use on endosome quantification (in HEK293T cells – Supplemental File 3 and in ECFCs – Supplemental File 4), WPB

quantification after Golgi ribbon disruption (Supplemental File 5) and after forskolin stimulation (Supplemental File 6) are also made available. To compare the CellProfiler measurements and validate these, manual scoring of cell count, cell surface area, WPB count, WPB length, and VWF and Rab27A intensity inside and outside the WPBs was performed using Fiji version 2.3.0 (13). Scoring was performed by using the built in scale and drawing regions of interest per cell and per WPB.

Statistical Analysis

Output data of the OrganelleProfiler pipeline was compared by Mann-Whitney U test if data was not normally distributed and unpaired T test with Welch's correction was performed on normally distributed data. Data of the OrganelleContentProfiler pipeline was compared with RM one way ANOVA with Geisser-Greenhouse correction. Data are presented as median with min/max boxplot. Results with p value < 0.05 were considered statistically significant. P values are indicated on the graphs in the figures. Data analyses were performed using GraphPad Prism 9.3.1 (GraphPad Software, San Diego, CA, USA).

Results

Development of OrganelleProfiler (OP) – Automated identification and quantification of nuclei, cells and secretory organelles

Described here are the modules used in the OrganelleProfiler pipeline for the identification and measurement of endothelial cells, their nuclei and WPBs. The most important parameters and how these can be adjusted for use on other tissues for each module are mentioned in Supplemental File 7. Full explanations of other variables are available from the help function within the CellProfiler software or from the user manual on the CellProfiler website. For the development of OrganelleProfiler we used confocal images from 33 ECFC clones from several healthy donors. These ECFCs have previously been classified into separate phenotypic groups based on cellular morphology and showed clear differences in expression of cell surface markers, proliferation and storage and secretion of VWF (6). Representative images of 1 clone of group 1 (top) and 1 clone of group 3 (bottom) ECFCs used for this study are shown in Figure 1. The CellProfiler modules that together form the OrganelleProfiler pipeline can be divided into 6 steps (Figure 2), which are described below.
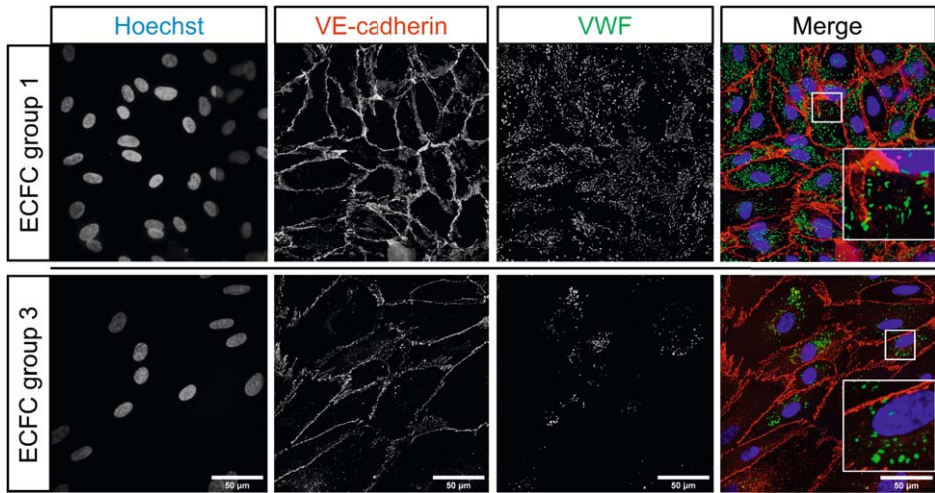
Figure 1. Representative images of healthy ECFC controls belonging to previously classified groups based on morphology (6). Group 1 ECFCs (top) and group 3 ECFCs (bottom) were stained with Hoechst (blue) and antibodies against VE-cadherin (red) and VWF (green). Scale bar represents 50 μm. Images were taken with a 63x objective.
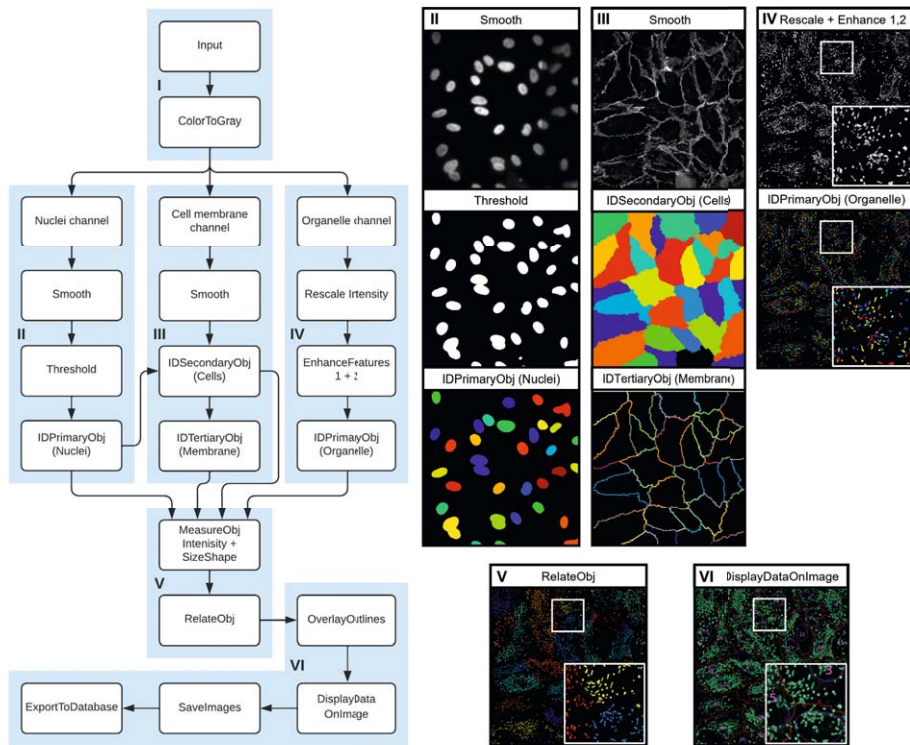
Figure 2. OrganelleProfiler: Quantitative and qualitative analysis of cells and cell secretory organelles. Left, flowchart of the modules within the OrganelleProfiler pipeline. I) Input of images and splitting of channels. II) Smoothing (top), thresholding (middle) and identification of the nuclei (bottom). Every different color indicates a different object. III) Smoothing of the cell membrane (top), identification of the cells (middle) and identification of cell membranes (bottom) as objects. IV) VWF signal rescaling and enhancement (top) and identification of WPB objects (bottom). V) Relating WPBs and Cells as child and parent respectively. Same colored objects indicate a relationship to the same cell. VI) Generated output image overlaying the outline of the nuclei (blue), cells (red), and WPBs (green) objects on the VWF channel. With the addition of the cell number (purple).

Step I – Input of images

Firstly, images of interest are imported into the software. In this example, 5 images from two groups of ECFCs were compared. Each image has 3 channels, 1 for the nuclei staining (Hoechst), one for cell membrane staining (VE-cadherin) and a third channel for organelle specific staining (VWF) (Figure 1). Channels are separated at this point so that each channel is processed separately in the following steps.

Step II, III and IV – Identification of nuclei, cell membranes, cells and organelles
Second, the nuclei staining signal is smoothed and a threshold is applied for the identification of the nuclei as objects. This object, together with the smoothed cell membrane staining signal is used in step III for the identification of the whole cell as secondary object. The nuclei are used as a starting point from which the object propagates outward in all directions until it encounters a secondary signal, in this case the smoothed cell membrane. A third object is generated using the cell object. This third object consists of only the cell membrane which is needed in the OrgannelleContentPipeline. In parallel to steps II and III, step IV uses the organelle staining signal for identification of the organelles. The signal is first rescaled and the speckle and neurite features are enhanced, which yields a better separation of organelles if they are located close to, or on top of, each other. After modification, the organelles are identified as the fourth object class.

Step V – Measurement and relating of objects
All objects that are generated in step II, III and IV are measured here. Size, shape and intensity, where relevant, is measured. Organelle objects are related to the nuclei and to the cell membrane in this step as well. This yields counts of secondary objects (organelles) per primary objects (cells) and distance of the secondary object to either the nuclei or the cell membrane. Measurements that we performed on the objects are eccentricity (as indicator for round or elongated WPB morphology), length of WPBs (maximum ferret diameter) and absolute as well as relative distance of WPBs to the nuclei and the cell membrane (Figure 3A).
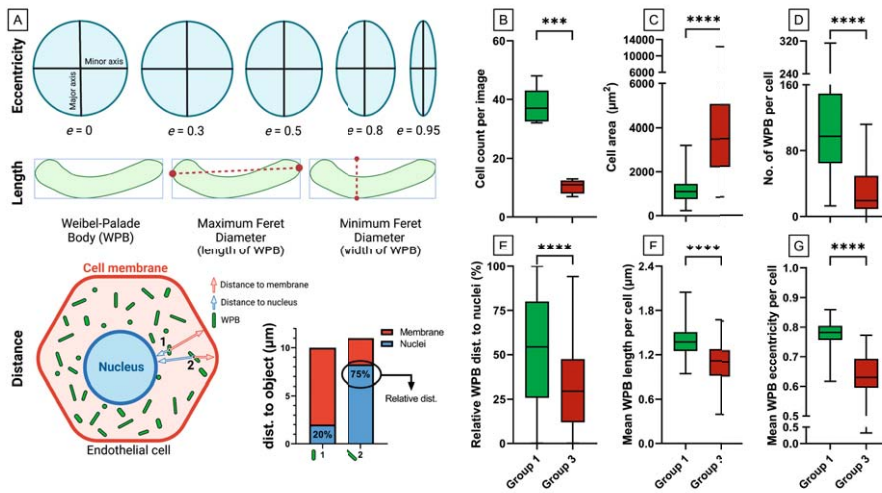
3

Figure 3. Quantitative and morphological differences between ECFC control groups.
Two previously classified ECFCs based on morphology (6), group 1 (green) and group 3 (red), were stained for Hoechst, VE-cadherin and VWF. Per control, 5 images were analyzed with the OrganelleProfiler pipeline (each 44100 µm^2 in size). A) Graphical representation of the measurements that were performed on the objects. Eccentricity (top), length of Weibel-Palade bodies (WPBs) measured as maximum ferret diameter (middle) and distance of WPBs to the nuclei and the cell membrane was measured (bottom). Relative distance of the WPB to the nucleus in the cell was calculated as 100% x (distance to nucleus) / (distance to nucleus + distance to cell membrane). B) Cell count per image. C) The cell area (µm^2) per cell of all 5 images pooled (n = 188 in group 1 and n = 52 in group 3). D) Number of WPBs per cell. E) Distance of the WPB to the nucleus relative to their position in the cell in percentage. F) Mean WPB length per cell in µm. G) Mean eccentricity of WPBs per cell. Data is shown as median with min/max boxplot. Mann-Whitney U test was performed on not normally distributed data (D and G). Unpaired T test with Welch's correction was performed on normally distributed data (B, C, E and F); *p<0.05 **p<0.01, ***p<0.001.

Step VI – Quality control and analysis of output

For quality control, all objects' outlines are overlaid on the VWF signal. This overlay allows the user to check whether the pipeline was accurate in the identification of objects. Cells are numbered so potential outliers can be easily identified and the pipeline can be adjusted if needed. The exported output can be used to quantify and perform qualitative analysis on images of interest.

Automated quantification using OrganelleProfiler revealed significant differences in cell count, cell area and number, size, shape and localization of WPBs between group 1 and group 3 ECFCs (Figure 3B-G). Figure 3B shows a significantly lower number of cells per image in group 3 (mean ± SD, 10.40 ± 2.40) compared to group 1 (37.60 ± 2.80)

(p=0.0003). Logically, as all ECFCs were confluent, we observed a larger mean cell area in group 3 (4016 ± 2445 µm^2) than in group 1 (1143 ± 516.60 µm^2) (Figure 3C) (p<0.0001). The total number of WPBs per image was lower in group 1 compared to group 3 (not shown). Additionally, the number of WPBs per cell was significantly lower in group 3 (30.92 ± 29.54) than in group 1 (107.30 ± 58.51) (p<0.0001) (Figure 3D). The distance of WPBs to the nuclei relative to their position in the cell was determined and shown in Figure 3E. The relative distance was significantly lower in group 3 ECFCs (32.31 ± 23.62%) when compared to group 1 (53 ± 30.10%) (p<0.0001) indicating that within the cell, WPBs were located closer to the nucleus in group 3 ECFCs. Finally, the mean WPB length was lower in group 3 (1.10 ± 0.27 µm) versus (1.38 ± 0.21 µm) in group 1 ECFCs (p<0.0001) and the WPBs were significantly more round in group 3 (0.63 ± 0.08)) versus (0.78 ± 0.04) (p<0.0001) (Figure 3F/G). The lower number of WPBs and the observation that they are smaller and rounder in group 3 when compared to group 1 could explain the decreased production and secretion of VWF observed previously (de Boer, JTH, 2020).

To further validate the quantitative data obtained from our automated OrganelleProfiler pipeline we also performed a manual quantification of several of these parameters using Fiji image analysis software, specifically the region of interest manager (13). One image of the group 1 ECFCs was used for the scoring. The manual scoring of the cells using the freehand selection resulted in 34 cells with a mean surface area of 1264 ± 497.93 µm^2. For three cells all WPBs were scored by measuring the longest distance in the WPB using a straight line. In these cells the manual scoring showed a mean WPB count of 117 ± 38.63 and a length of 1.57 ± 0.09 µm. All measurements were compared with the CellProfiler measurements on the same image and none of the results differed significantly. Taken together, we can conclude that both measurements with CellProfiler and Fiji are comparable and thus CellProfiler can be used to accurately measure cells and organelles.

Validation and application of OrganelleProfiler
Identification of HEK293T cells and early endosomes
To demonstrate the versatility of the OrganelleProfiler pipeline, we extended our analyses to a different type of organelle (early endosome, visualized by staining for early endosome antigen 1, EEA1) and a different cell type (HEK293T). Representative images of ECFCs and HEK293T cells and the analyzed output of the OrganelleProfiler are shown in Figure 4A. The OrganelleProfiler was used to analyze three tile scans of each condition. Figure 4B shows significantly more HEK293T cells per image (1539 ± 82.71) than ECFCs (359.30 ± 4.16) (p=0.0016) which were also smaller (397.8 ± 150 µm^2) than ECFCs (1793 ± 866.3 µm^2) (Figure 4C) (p<0.0001). The number of early endosomes per cell was slightly lower in HEK293T cells (39.27 ± 16.22) compared to ECFCs (63.30 ± 41.02) (p<0.0001) (Figure 4D). The relative distance of the early endosomes to the nuclei (Figure 4E) was higher in the

3

HEK293T cells (45.34 ± 8.29%) when compared to ECFCs (40.05 ± 12.70%) (p<0.0001). Finally, the mean early endosome eccentricity is slightly higher in HEK293T cells (0.59 ± 0.05) versus (0.58 ± 0.04) in ECFCs (p<0.0001) (Figure 4F). Comparatively, the early endosomes are clearly rounder when compared to WPBs (0.78 ± 0.04, indicated by the red dotted line, data from Figure 3G) which are more elongated organelles.
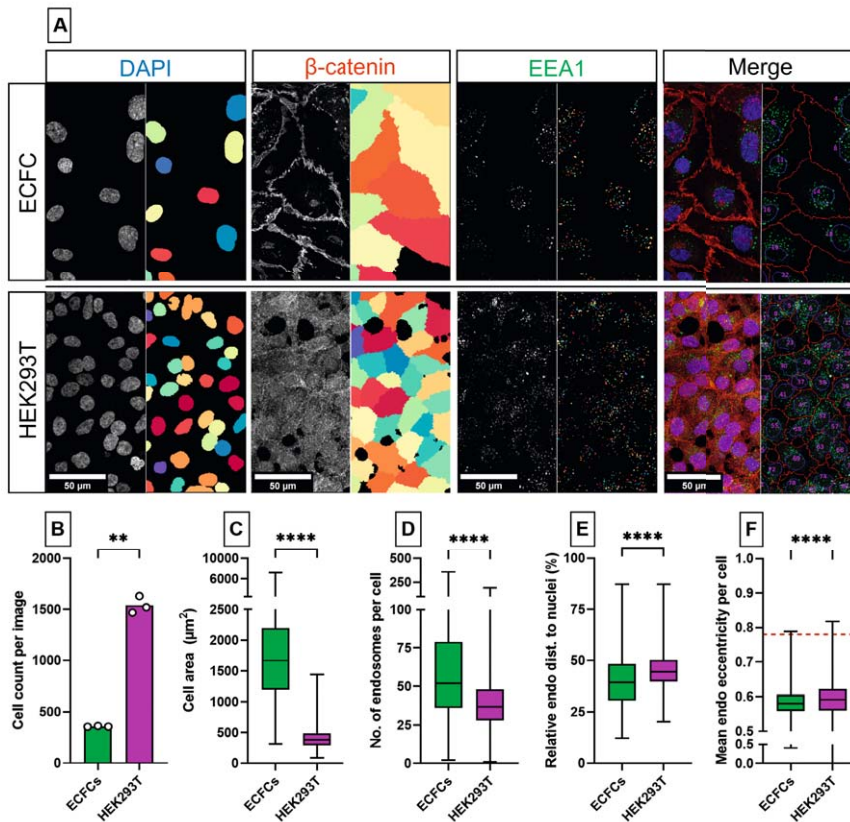

Figure 4. Quantitative and morphological differences between early endosomes in ECFCs and HEK293T cells. A) Representative images of ECFC (top) and HEK293T (bottom) cells where each panel shows the raw confocal image (left) and the identified object in Cellprofiler (right). Every different color indicates a different object. Cells were stained with DAPI (blue) and antibodies against β-catenin (red) and EEA1 (green). Scale bar represents 50 μm. Images were taken with a Leica Stellaris 5 LIA fitted with a 63x objective. Per cell type, 3 tile scans (each 754630 μm² in size) were analyzed with the OrganelleProfiler pipeline. B) Cell count per image. C) The cell area (μm²) per cell of all 3 tile scans pooled (n = 1078 ECFCs and n = 4618 HEK293T cells). D) Number of endosomes per cell. E) Mean relative distance of the endosome to the nucleus per cell. F) Mean eccentricity of endosomes per cell. Data is shown as median with min/max boxplot. Dashed red line represents mean eccentricity of WPBs as determined in Figure 3G. Mann-Whitney U test was performed on not normally distributed data (C,D,E,F). Unpaired T test with Welch's correction was performed on normally distributed data (B); **p<0.01, ***p<0.001, ****p<0.0001.

WPB shortening after Golgi ribbon disruption and perinuclear clustering after stimulation

WPB length directly relates to the integrity of the Golgi ribbon: fragmented Golgi ribbons generate small WPBs while the longest WPBs require an extended, intact Golgi ribbon (3, 14-16). Pharmacological inhibition of microtubules using nocodazole can be used to unlink Golgi ribbons (17) and this has been shown to reduce the size of newly generated WPBs (14, 18). We used OrganelleProfiler to quantify the reduction of WPB length in ECFCs that were treated for 46 hours with vehicle (DMSO, control) or 2 µg/ml nocodazole. Staining for VWF and the trans-Golgi network marker TGN46 revealed a clear disruption of the Golgi in nocodazole-treated cells (Figure 5A). The OrganelleProfiler was used to analyze three tile scans of each condition. Nocodazole exposure caused a lower cell count per image (Figure 5B) (n=184.7 ± 5.51 versus n=553 ± 36.43, p=0.0027) with larger surface area (2859 ± 1314 µm^2) than control ECFCs (1673 ± 641.6 µm^2) (Figure 5C) (p<0.0001). In the nocodazole treated cells we observed significantly rounder (nocodazole: 0.76 ± 0.06 vs control: 0.87 ± 0.02; p<0.0001) and shorter WPBs (nocodazole: 1.17 µm ± 0.18 vs. control: 1.54 ± 0.17 µm; p<0.0001) compared to the control cells (Figure 5D and E). The relative distance of the WPBs to the nuclei (Figure 5E) was slightly higher after nocodazole exposure (62.25 ± 13.77%) when compared to control (60.18 ± 8.17%) (p<0.0018).
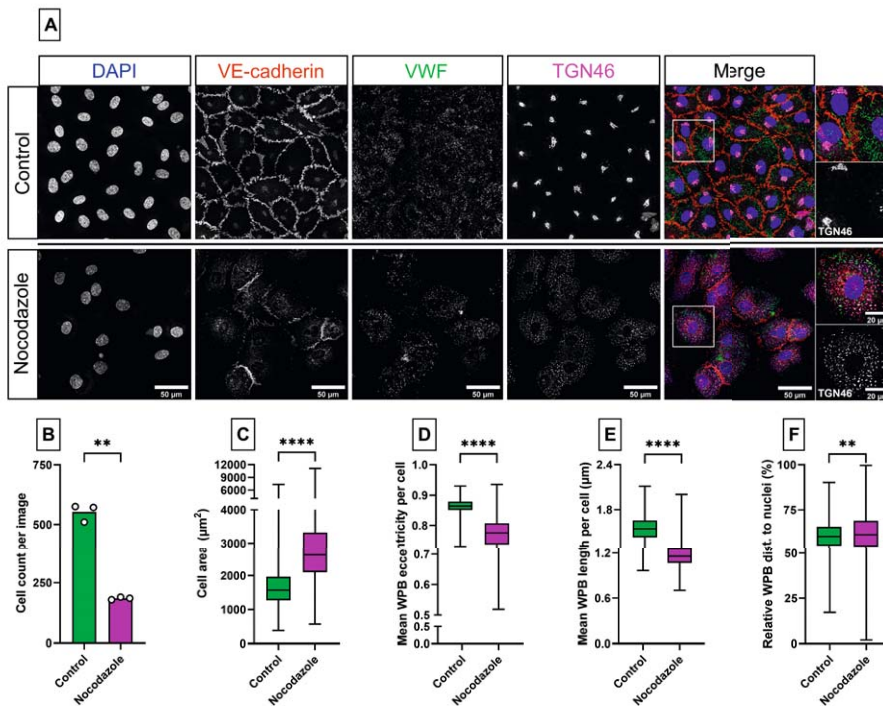
3

Figure 5. Microtubule disruption leads to Golgi fragmentation and smaller and rounder WPBs. A) Representative images of ECFCs treated for 46 hours with vehicle (control, top) or 2 μg/ml nocodazole (bottom). Cells were stained with DAPI (blue) and antibodies against VE-cadherin (red), VWF (green) and TGN46 (magenta). Scale bar represents 50 μm and 20 μm in the zoom in. Images were taken with a 63x objective. Per cell type, 3 tile scans (each 936054 μm^2 in size) were analyzed with the OrganelleProfiler pipeline. B) Cell count per image. C) The cell area (μm^2) per cell of all 3 tile scans pooled (n = 1659 in the control and n = 554 in the nocodazole treated cells). D) Mean eccentricity of WPBs per cell. E) Mean length (μm) of WPBs per cell F) Mean relative distance of the WPBs to the nucleus per cell. Data is shown as median with min/max boxplot. Mann-Whitney U test was performed on not normally distributed data (C,D,E,F). Unpaired T test with Welch's correction was performed on normally distributed data (B); **$p<0.01$, ***$p<0.001$, ****$p<0.0001$.

It has previously been shown that, upon activation with cAMP-mediated agonists such as epinephrine or forskolin, endothelial cells cluster a subset of their WPBs at the microtubule organizing center (MTOC) via retrograde microtubular transport that depends on the minus-end motor protein dynein (19, 20). We used OrganelleProfiler to quantify the reorganization of WPBs in forskolin-stimulated ECFCs (Figure 6A). Quantitative data gathered from one tile scan per condition shows that the per cell mean relative distance to the nucleus, which is directly adjacent to the MTOC and can therefore be used as a surrogate reference point for clustered WPBs, is lower in

forskolin-treated cells (50.67 ± 14.76%, n=352 cells) than in untreated cells (58.15 ± 10.22%, n=537 cells) (Figure 6B, top). This indicates that in forskolin-treated cells, WPBs have on average moved towards the nucleus and thus into the direction of the MTOC. Also, when quantified on a single organelle basis, we see a shift towards lower relative distance to the nucleus in forskolin-treated cells (45.32 ± 31.39%, n=17241 WPBs) compared with untreated cells (54.03 ± 30.77%, n=21866 WPBs) (Figure 6B, bottom).
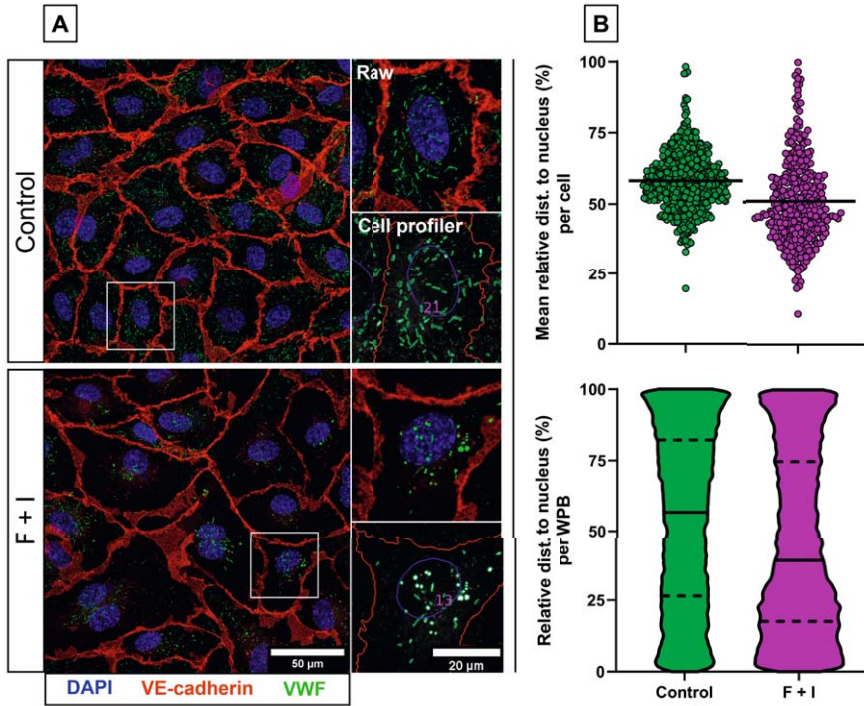

Figure 6. Perinuclear clustering of WPBs after cAMP-mediated signaling in ECFCs. A) Representative images of ECFCs treated for 30 minutes with vehicle (control, top) or 10 uM Forskolin and 100 uM IBMX (F+I, bottom). Cells were stained with DAPI (blue) and antibodies against VE-cadherin (red) and VWF (green). Scale bar represents 50 μm and 20 μm in the zoom in. Images were taken with a 63x objective. Per condition, 1 tile scan (970221 μm² in size) was analyzed with the OrganelleProfiler pipeline. B) Mean relative distance of the WPBs to the nucleus per cell (top) (n = 537 in the control and n = 352 in the stimulated ECFCs) and per WPB (bottom) shown as violin plot (n= 21866 for the control and n=17241 for the stimulated ECFCs). The black bar indicates the median with quartiles.

OrganelleContentProfiler (OCP) – Automated measurement of proteins in secretory organelles

The OrganelleContentProfiler pipeline is an addition to the OrganelleProfiler pipeline. By adding 4 extra steps, secondary proteins of interest in, on or outside the organelle can be measured. For this purpose we analyzed the presence of Rab27A, a small GTPase that promotes WPB exocytosis and that is recruited to the WPB membrane during the maturation of these organelles after their separation from the Golgi complex (9, 10, 21). We also determined, as a control, the presence of protein disulfide isomerase (PDI), a marker for the endoplasmic reticulum which should not show specific localization in or on the WPBs (5, 15). Figure 7 shows example images of Rab27A as well as PDI co-staining in group 1 healthy donor ECFCs that were used in this pipeline. The CellProfiler modules that together form the OrganelleContentProfiler pipeline can be divided into 4 steps (Figure 8), which are described below. Further details on every module are described in Supplemental File 7.
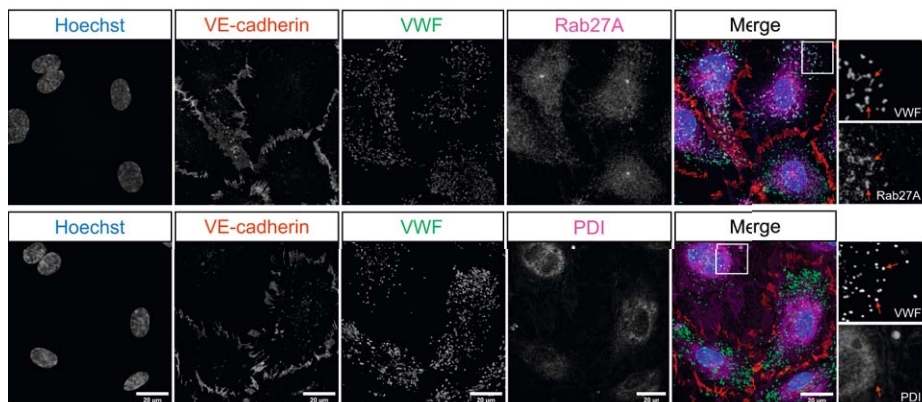

Figure 7. Representative images of one healthy group 1 ECFC control belonging to previously classified groups based on morphology (6). Cells were stained for Hoechst (blue), VE-cadherin (red), VWF (green) and Rab27A (top) or PDI (bottom). Scale bar represents 20 μm. Images were taken with a 63x objective. Red arrows indicate WPBs as identified in the VWF channel and the same location in the Rab27A or PDI channel.
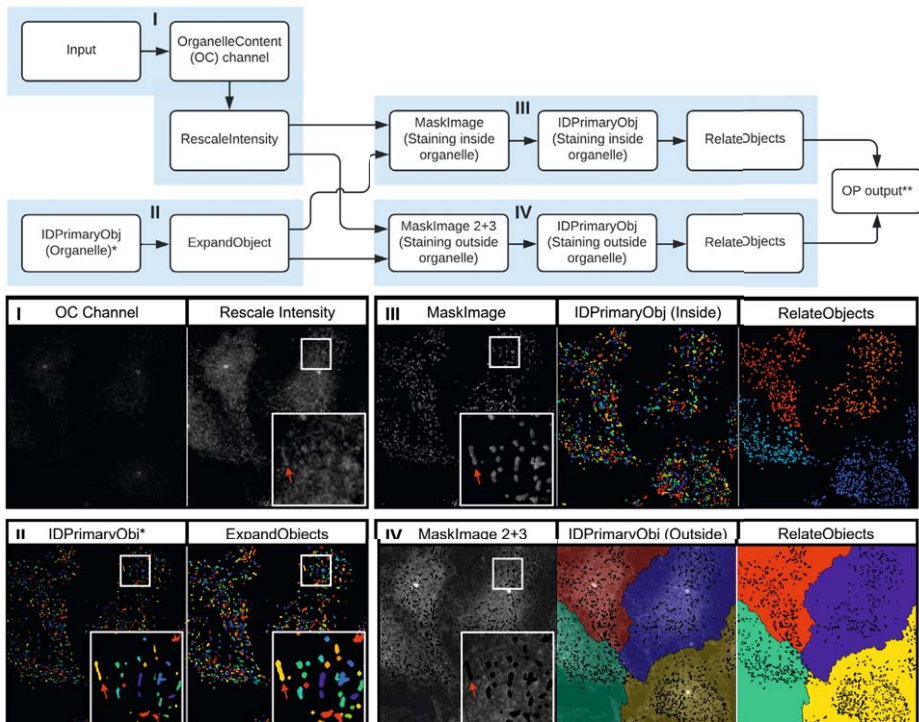
Figure 8. OrganelleContentProfiler: Quantitative and qualitative analysis of other organelle proteins. Top, flowchart of the modules within the OrganelleContentProfiler pipeline. I) Input of Rab27A (Organelle content) channel and rescaling of this channel. II) Input of primary object (Organelle) (left) and expansion of this object (right). III) Masking of the Rab27A channel using the Expanded organelle objects to leave only Rab27A signal inside the organelle (left). Identification of the Rab27A signal per WPB as object (middle) and relating these objects to the cells as child and parent respectively (right). IV) Masking of the Rab27A channel using the Expanded organelle objects to leave only Rab27A signal outside the organelle (left). Identification of the Rab27A signal in the cell as object without the WPBs (middle) and relating these objects to the cells as child and parent respectively (right). * Identified in step IV of the OrganelleProfiler pipeline (Figure 2). ** Pipeline continues with step V and VI from the OrganelleProfiler pipeline.

Step I – Input of an additional channel
Similarly to the OrganelleProfiler, images are imported into the software. In this example, images have one additional channel containing the staining for either Rab27A or PDI. Again, channels are separated and the fourth channel is rescaled in order to view the channel in the final quality control.

Step II – Import of organelle object identified in the OrganelleProfiler pipeline
In this step, the organelle object as identified in the OrganelleProfiler pipeline is modified. The objects are initially identified using the staining for VWF, which is a

cargo protein that is contained within the organelle. The secondary protein of interest, Rab27A, is a membrane protein that is located on the cytoplasmic face of the WPB membrane. To ensure full encapsulation of the Rab27A signal the object is therefore expanded by 2 pixels in all directions.

Step III and IV – Identification of the secondary protein of interest "inside" and outside the organelle

In these parallel steps, the expanded organelle objects and the rescaled secondary staining channel are used. The expanded objects are used as a mask to remove all signal of the Rab27A or PDI staining outside the organelle (step III) and inside the organelle (step IV). The remaining signal is then identified as object, resulting in two new objects containing the signal inside the organelles and outside the organelles respectively. These new objects are processed according to step V from the OrganelleProfiler including the measurements, relating, quality control and export.

Step V and VI – Measurements, quality control and analysis of results

In the OrganelleContentProfiler pipeline, different stainings on the same ECFC control are compared. In addition to the output from the OrganelleProfiler, the OrganelleContentProfiler provides measurements of the intensity of a secondary signal inside the organelle. Furthermore, it can quantify the cytoplasmic intensity values outside of the organelle which can be used for correction of the "inside" organelle signal. Signal intensity is noted as arbitrary intensity units (A.U.) as microscopes are not calibrated to an absolute scale.

We first confirmed that the number of WPBs quantified using OrganelleContentProfiler does not depend on the co-staining used (Rab27A: 204.8 ± 70.48; PDI: 146, ± 56.38; p=0.24) (Figure 9A). ECFCs were stained with Hoechst and with antibodies against VE-cadherin, VWF and Rab27A or PDI. Figure 9B shows the A.U. inside and outside organelles and the A.U. inside the organelle corrected for the outside value. First, the VWF A.U. was analyzed as a measurement of a protein that is located predominantly in the WPB. The results show that the VWF A.U. values outside the WPBs was nearly zero (0.00076 ± 0.00033) and differed significantly from the inside A.U. (0.028 ± 0.0040) (p=0.0016) indicating that VWF is almost exclusively present in WPBs. Secondly, it was determined that the Rab27A staining shows a significantly higher A.U. inside (0.081 ± 0.0085) the WPBs when compared to the outside measurement (0.052 ± 0.0041) (p=0.0062). From this it can be concluded that part of the Rab27A protein is present in or on the WPB. Finally, the A.U. of the PDI staining was analyzed. PDI is only present inside the endoplasmic reticulum and should not yield increased A.U. inside the WPB. Indeed, the A.U. inside (0.074 ± 0.016) and outside (0.062 ± 0.0082) the organelle were

similar (p=0.20), indicating that PDI is not located specifically in or on WPBs. Once more, to validate the quantitative data obtained by CellProfiler, we also performed a manual scoring using Fiji for the A.U. of the Rab27A and VWF staining inside and outside of all WPBs (n=199) in one cell. We observed that the results determined manually using Fiji (A.U. VWF inside = 0.039, VWF outside = 0.000029; Rab27A inside = 0.094, Rab27A outside = 0.053) lie within the same range as those determined by CellProfiler. This shows that the OrganelleContentProfiler can determine organelle specific stainings and measure the intensity of the staining corrected for the cytoplasmic value.
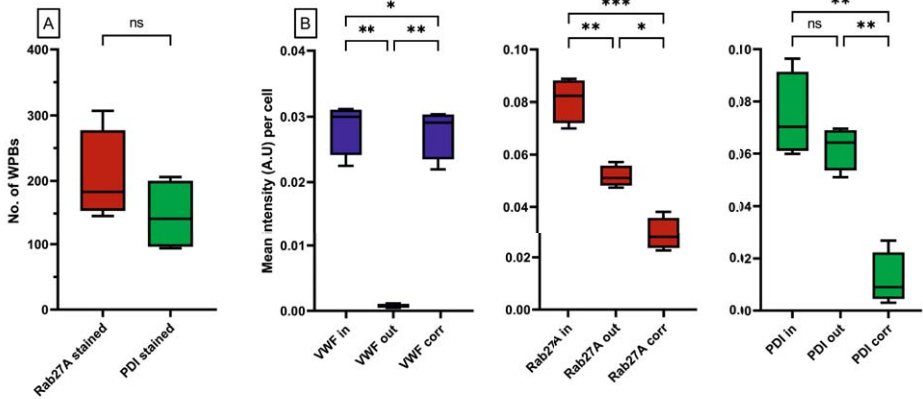

Figure 9. Quantification of signal intensity inside cell organells. A group 1 ECFC control as defined previously (6) was stained with Hoechst and with antibodies against VE-cadherin, VWF and PDI or Rab27A. One image (12769 µm^2) per staining was analyzed using the OrganelleContentProfiler pipeline. A) Both images had the same number of cells (n=4) and roughly the same number of WPBs. B) the mean intensity in arbitrary intensity units (A.U.) per cell for the PDI (left), Rab27A (middle) and VWF (right) staining. Each graph shows the measured mean intensity inside (in) the WPBs, outside (out) the WPBs and the intensity inside the WPB after correcting for the out signal (corr). Data is shown as median with min/max boxplot. RM one way ANOVA was performed with Geisser-Greenhouse correction; *p<0.05 **p<0.01, ***p<0.001.

Discussion

Quantifying large numbers of organelles is challenging due to the density and morphological heterogeneity of the organelles. The pipelines described here can be used to overcome these challenges and can provide organelle analysis in great detail on a larger scale. The OrganelleProfiler allows for measurement of cell and nucleus quantity and shape, and organelle quantity, shape, size and location within the cell. The organelles are also related to the cells which allows for cell-by-cell analysis. This information can be used to determine differences between a heterogeneous cell

population or between patient and control cells. The OrganelleProfiler pipeline has shown significant differences between group 1 and group 3 ECFC controls based on only 5 images. Moreover, we were able to quantitatively determine differences in WPB length upon treatment with cytoskeletal drugs and differences in intracellular localization after induction of retrograde transport of WPBs. Once optimized for a set of images, the pipeline can analyze thousands of cells and hundreds of thousands of organelles within hours without potential bias associated with manual image processing and quantification. As shown with the early endosome staining, it is possible to adjust the pipeline to quantify other cell types and organelles. The pipeline was able to quantify differences between ECFCs and HEK293T cells and showed clear differences in eccentricity of the elongated WPBs compared to the round early endosomes.

With the OrganelleContentProfiler, secondary organelle markers can be measured and quantified. We showed 3 stainings of proteins with different localizations; PDI, which is only present on the endoplasmic reticulum, Rab27A which is present in the cytoplasm, but is also trafficked to the WPBs, and VWF which is mostly present in WPBs. Using the OrganelleContentProfiler pipeline we were able to quantify these stainings and determine the localization of these proteins. It is also possible to measure other organelle stainings at the same time by duplicating modules 3 to 8 of this pipeline and adjusting these for the additional channels.

Finetuning of the smoothing, thresholds and enhancement of the signal is necessary to ensure correct identification of objects. For every image set, a balance must be found to prevent over and under segmentation of organelles. Despite optimization, perfect segmentation of organelles is not always possible, especially in areas where organelles are crowded together. These imperfections may lead to incorrect identification of organelles, which could play out as underestimations of WPB numbers or overestimation of WPB dimensions. However, as all images are analyzed by the same pipeline, this error is expected to occur to a similar extent in all samples. One point of improvement on the OrganelleContentProfiler pipeline could be the correction of the organelle secondary staining with the intensity levels directly surrounding the organelle instead of the mean intensity in the entire cytoplasm. This was not possible within the CellProfiler software but could be done in data processing afterwards using the MeasureObjectIntensityDistribution module and relating this to the distance of WPBs to the nucleus (7).

A comparison with manual scoring using Fiji was performed to check the validity of the results generated by our automated pipelines. We generally found that the results obtained with OrganelleProfiler and OrganelleContentProfiler correspond very

well with manual quantifications using Fiji, although subtle differences were found for two parameters. First, the maximum ferret diameter is calculated based on the smallest convex hull that is created around the WPB. The manual scoring measured the length of the WPB in a line and not as the inside of a convex hull. This could cause the slight difference in length as measured between CellProfiler and Fiji. Second, VWF and Rab27A intensities inside WPBs as determined by manual scoring was slightly higher than from the OrganelleContentProfiler measurements. Possibly, the outlines that were drawn around WPBs manually were more strict than those generated by OrganelleContentProfiler, because the human eye is less capable at detecting the very small changes in signal intensity near the edges of the organelles. As such, the signal intensities in these edges may have not been included in the manual analysis, resulting in a higher mean value per WPB.

To conclude, the OrganelleProfiler and OrganelleContentProfiler pipelines provide powerful, high-processing quantitative tools for analysis of cell and organelle count, size, shape, location and content. These pipelines were created with the purpose of analyzing morphometric parameters of WPBs in endothelial cells, but as shown for the HEK293T cells and early endosomes, they can be easily adjusted for use on different cell types or organelles. This can be especially useful for analysis of large datasets where manual quantification of organelle parameters would be unfeasible.

3

Acknowledgements

References

1. Schillemans M, Karampini E, Kat M, Bierings R. Exocytosis of Weibel-Palade bodies: how to unpack a vascular emergency kit. J Thromb Haemost. 2019;17(1):6-18.
2. Valentijn KM, Sadler JE, Valentijn JA, Voorberg J, Eikenboom J. Functional architecture of Weibel-Palade bodies. Blood. 2011;117(19):5033-43.
3. Kat M, Margadant C, Voorberg J, Bierings R. Dispatch and delivery at the ER-Golgi interface: how endothelial cells tune their hemostatic response. FEBS J. 2022;289(22):6863-70.
4. Valentijn KM, Eikenboom J. Weibel-Palade bodies: a window to von Willebrand disease. J Thromb Haemost. 2013;11(4):581-92.
5. de Jong A, Weijers E, Dirven R, de Boer S, Streur J, Eikenboom J. Variability of von Willebrand factor-related parameters in endothelial colony forming cells. J Thromb Haemost. 2019;17(9):1544-54.
6. de Boer S, Bowman M, Notley C, Mo A, Lima P, de Jong A, et al. Endothelial characteristics in healthy endothelial colony forming cells; generating a robust and valid ex vivo model for vascular disease. J Thromb Haemost. 2020;18(10):2721-31.
7. Stirling DR, Swain-Bowden MJ, Lucas AM, Carpenter AE, Cimini BA, Goodman A. CellProfiler 4: improvements in speed, utility and usability. BMC Bioinformatics. 2021;22(1):433.
8. Hannah MJ, Hume AN, Arribas M, Williams R, Hewlett LJ, Seabra MC, et al. Weibel-Palade bodies recruit Rab27 by a content-driven, maturation-dependent mechanism that is independent of cell type. J Cell Sci. 2003;116(Pt 19):3939-48.
9. Bierings R, Hellen N, Kiskin N, Knipe L, Fonseca AV, Patel B, et al. The interplay between the Rab27A effectors Slp4-a and MyRIP controls hormone-evoked Weibel-Palade body exocytosis. Blood. 2012;120(13):2757-67.
10. Kat M, Bürgisser PE, Janssen H, De Cuyper IM, Conte IL, Hume AN, et al. GDP/GTP exchange factor MADD drives activation and recruitment of secretory Rab GTPases to Weibel-Palade bodies. Blood Adv. 2021;5(23):5116-27.
11. Schillemans M, Kat M, Westeneng J, Gangaev A, Hofman M, Nota B, et al. Alternative trafficking of Weibel-Palade body proteins in CRISPR/Cas9-engineered von Willebrand factor-deficient blood outgrowth endothelial cells. Res Pract Thromb Haemost. 2019;3(4):718-32.
12. van Hooren KW, van Breevoort D, Fernandez-Borja M, Meijer AB, Eikenboom J, Bierings R, et al. Phosphatidylinositol-3,4,5-triphosphate-dependent Rac exchange factor 1 regulates epinephrine-induced exocytosis of Weibel-Palade bodies. J Thromb Haemost. 2014;12(2):273-81.
13. Schindelin J, Arganda-Carreras I, Frise E, Kaynig V, Longair M, Pietzsch T, et al. Fiji: an open-source platform for biological-image analysis. Nature Methods. 2012;9(7):676-82.
14. Ferraro F, Kriston-Vizi J, Metcalf DJ, Martin-Martin B, Freeman J, Burden JJ, et al. A two-tier Golgi-based control of organelle size underpins the functional plasticity of endothelial cells. Dev Cell. 2014;29(3):292-304.
15. Kat M, Karampini E, Hoogendijk AJ, Bürgisser PE, Mulder AA, Van Alphen FPJ, et al. Syntaxin 5 determines Weibel-Palade body size and von Willebrand factor secretion by controlling Golgi architecture. Haematologica. 2022;107(8):1827-39.
16. Karampini E, Bürgisser PE, Olins J, Mulder AA, Jost CR, Geerts D, et al. Sec22b determines Weibel-Palade body length by controlling anterograde ER-Golgi transport. Haematologica. 2021;106(4):1138-47.

17. Thyberg J, Moskalewski S. Microtubules and the organization of the Golgi complex. Exp Cell Res. 1985;159(1):1-16.
18. Ferraro F, Patella F, Costa JR, Ketteler R, Kriston-Vizi J, Cutler DF. Modulation of endothelial organelle size as an antithrombotic strategy. Journal of Thrombosis and Haemostasis. 2020;18(12):3296-308.
19. Rondaij MG, Bierings R, Kragt A, Gijzen KA, Sellink E, van Mourik JA, et al. Dynein-dynactin complex mediates protein kinase A-dependent clustering of Weibel-Palade bodies in endothelial cells. Arterioscler Thromb Vasc Biol. 2006;26(1):49-55.
20. van Agtmaal EL, Bierings R, Dragt BS, Leyen TA, Fernandez-Borja M, Horrevoets AJG, et al. The Shear Stress-Induced Transcription Factor KLF2 Affects Dynamics and Angiopoietin-2 Content of Weibel-Palade Bodies. PLOS ONE. 2012;7(6):e38399.
21. Zografou S, Basagiannis D, Papafotika A, Shirakawa R, Horiuchi H, Auerbach D, et al. A complete Rab screening reveals novel insights in Weibel-Palade body exocytosis. J Cell Sci. 2012;125(Pt 20):4780-90.
22. Cnossen MH, van Moort I, Reitsma SH, de Maat MPM, Schutgens REG, Urbanus RT, et al. SYMPHONY consortium: Orchestrating personalized treatment for patients with bleeding disorders. J Thromb Haemost. 2022;20(9):2001-11.
23. Hordijk S, Carter T, Bierings R. A new look at an old body: molecular determinants of Weibel-Palade body composition and VWF exocytosis. J Thromb Haemost. 2024.
24. Murray EW, Lillicrap D. von Willebrand disease: pathogenesis, classification, and management. Transfus Med Rev. 1996;10(2):93-110.
25. Leebeek FWG, Eikenboom JCJ. Von Willebrand's Disease. New England Journal of Medicine. 2016;375(21):2067-80.
26. Lin Y, Weisdorf DJ, Solovey A, Hebbel RP. Origins of circulating endothelial cells and endothelial outgrowth from blood. J Clin Invest. 2000;105(1):71-7.
27. van den Biggelaar M, Bouwens EA, Kootstra NA, Hebbel RP, Voorberg J, Mertens K. Storage and regulated secretion of factor VIII in blood outgrowth endothelial cells. Haematologica. 2009;94(5):670-8.
28. Berber E, James PD, Hough C, Lillicrap D. An assessment of the pathogenic significance of the R924Q von Willebrand factor substitution. J Thromb Haemost. 2009;7(10):1672-9.
29. Groeneveld DJ, van Bekkum T, Dirven RJ, Wang JW, Voorberg J, Reitsma PH, et al. Angiogenic characteristics of blood outgrowth endothelial cells from patients with von Willebrand disease. J Thromb Haemost. 2015;13(10):1854-66.
30. Randi AM, Laffan MA. Von Willebrand factor and angiogenesis: basic and applied issues. J Thromb Haemost. 2017;15(1):13-20.
31. Starke RD, Ferraro F, Paschalaki KE, Dryden NH, McKinnon TA, Sutton RE, et al. Endothelial von Willebrand factor regulates angiogenesis. Blood. 2011;117(3):1071-80.
32. Starke RD, Paschalaki KE, Dyer CE, Harrison-Lavoie KJ, Cutler JA, McKinnon TA, et al. Cellular and molecular basis of von Willebrand disease: studies on blood outgrowth endothelial cells. Blood. 2013;121(14):2773-84.
33. Wang JW, Bouwens EA, Pintao MC, Voorberg J, Safdar H, Valentijn KM, et al. Analysis of the storage and secretion of von Willebrand factor in blood outgrowth endothelial cells derived from patients with von Willebrand disease. Blood. 2013;121(14):2762-72.
34. Galili T, O'Callaghan A, Sidi J, Sievert C. heatmaply: an R package for creating interactive cluster heatmaps for online publishing. Bioinformatics. 2017;34(9):1600-2.

3

35.   Ashburner M, Ball CA, Blake JA, Botstein D, Butler H, Cherry JM, et al. Gene Ontology: tool for the unification of biology. Nature Genetics. 2000;25(1):25-9.

36.   Consortium TGO, Aleksander SA, Balhoff J, Carbon S, Cherry JM, Drabkin HJ, et al. The Gene Ontology knowledgebase in 2023. Genetics. 2023;224(1).

37.   Laan SNJ, Dirven RJ, Bürgisser PE, Eikenboom J, Bierings R. Automated segmentation and quantitative analysis of organelle morphology, localization and content using CellProfiler. PLoS One. 2023;18(6):e0278009.

38.   Goncharov NV, Popova PI, Avdonin PP, Kudryavtsev IV, Serebryakova MK, Korf EA, et al. Markers of Endothelial Cells in Normal and Pathological Conditions. Biochem (Mosc) Suppl Ser A Membr Cell Biol. 2020;14(3):167-83.

39.   Dejana E, Hirschi KK, Simons M. The molecular basis of endothelial cell plasticity. Nature Communications. 2017;8(1):14361.

40.   Yang J, Antin P, Berx G, Blanpain C, Brabletz T, Bronner M, et al. Guidelines and definitions for research on epithelial–mesenchymal transition. Nature Reviews Molecular Cell Biology. 2020;21(6):341-52.

41.   Reimand J, Isserlin R, Voisin V, Kucera M, Tannus-Lopes C, Rostamianfar A, et al. Pathway enrichment analysis and visualization of omics data using g:Profiler, GSEA, Cytoscape and EnrichmentMap. Nature Protocols. 2019;14(2):482-517.

42.   Medina RJ, O'Neill CL, O'Doherty TM, Wilson SE, Stitt AW. Endothelial progenitors as tools to study vascular disease. Stem Cells Int. 2012;2012:346735.

43.   Bowman M, Casey L, Selvam SN, Lima PDA, Rawley O, Hinds M, et al. von Willebrand factor propeptide variants lead to impaired storage and ER retention in patient-derived endothelial colony-forming cells. J Thromb Haemost. 2022;20(7):1599-609.

44.   Selvam SN, Casey LJ, Bowman ML, Hawke LG, Longmore AJ, Mewburn J, et al. Abnormal angiogenesis in blood outgrowth endothelial cells derived from von Willebrand disease patients. Blood Coagul Fibrinolysis. 2017;28(7):521-33.

45.   Tien TY, Wu YJ, Su CH, Hsieh CL, Wang BJ, Lee YN, et al. Pannexin 1 Modulates Angiogenic Activities of Human Endothelial Colony-Forming Cells Through IGF-1 Mechanism and Is a Marker of Senescence. Arterioscler Thromb Vasc Biol. 2023;43(10):1935-51.

46.   Sanchez-Duffhues G, Orlova V, ten Dijke P. In Brief: Endothelial-to-mesenchymal transition. The Journal of Pathology. 2016;238(3):378-80.

47.   Kalluri R, Weinberg RA. The basics of epithelial-mesenchymal transition. J Clin Invest. 2009;119(6):1420-8.

48.   Maleszewska M, Moonen JR, Huijkman N, van de Sluis B, Krenning G, Harmsen MC. IL-1β and TGFβ2 synergistically induce endothelial to mesenchymal transition in an NFκB-dependent manner. Immunobiology. 2013;218(4):443-54.

49.   Romero LI, Zhang DN, Herron GS, Karasek MA. Interleukin-1 induces major phenotypic changes in human skin microvascular endothelial cells. J Cell Physiol. 1997;173(1):84-92.

50.   Kutikhin AG, Tupikin AE, Matveeva VG, Shishkova DK, Antonova LV, Kabilov MR, et al. Human Peripheral Blood-Derived Endothelial Colony-Forming Cells Are Highly Similar to Mature Vascular Endothelial Cells yet Demonstrate a Transitional Transcriptomic Signature. Cells. 2020;9(4).

51.   Yoshimatsu Y, Kimuro S, Pauty J, Takagaki K, Nomiyama S, Inagawa A, et al. TGF-beta and TNF-alpha cooperatively induce mesenchymal transition of lymphatic endothelial cells via activation of Activin signals. PLOS ONE. 2020;15(5):e0232356.

52. Hulshoff MS, Xu X, Krenning G, Zeisberg EM. Epigenetic Regulation of Endothelial-to-Mesenchymal Transition in Chronic Heart Disease. Arteriosclerosis, Thrombosis, and Vascular Biology. 2018;38(9):1986-96.

53. Tura O, Skinner EM, Barclay GR, Samuel K, Gallagher RC, Brittan M, et al. Late outgrowth endothelial cells resemble mature endothelial cells and are not derived from bone marrow. Stem Cells. 2013;31(2):338-48.

54. Toshner M, Dunmore BJ, McKinney EF, Southwood M, Caruso P, Upton PD, et al. Transcript analysis reveals a specific HOX signature associated with positional identity of human endothelial cells. PLoS One. 2014;9(3):e91334.

55. Potente M, Mäkinen T. Vascular heterogeneity and specialization in development and disease. Nature Reviews Molecular Cell Biology. 2017;18(8):477-94.

56. Lin Y, Banno K, Gil CH, Myslinski J, Hato T, Shelley WC, et al. Origin, prospective identification, and function of circulating endothelial colony-forming cells in mice and humans. JCI Insight. 2023;8(5).

57. Sánchez-Duffhues G, García de Vinuesa A, van de Pol V, Geerts ME, de Vries MR, Janson SG, et al. Inflammation induces endothelial-to-mesenchymal transition and promotes vascular calcification through downregulation of BMPR2. J Pathol. 2019;247(3):333-46.

58. Rieder F, Kessler SP, West GA, Bhilocha S, de la Motte C, Sadler TM, et al. Inflammation-induced endothelial-to-mesenchymal transition: a novel mechanism of intestinal fibrosis. Am J Pathol. 2011;179(5):2660-73.

59. Derada Troletti C, Fontijn RD, Gowing E, Charabati M, van Het Hof B, Didouh I, et al. Inflammation-induced endothelial to mesenchymal transition promotes brain endothelial cell dysfunction and occurs during multiple sclerosis pathophysiology. Cell Death & Disease. 2019;10(2):45.

60. Medina RJ, O'Neill CL, O'Doherty TM, Chambers SE, Guduric-Fuchs J, Neisen J, et al. Ex vivo expansion of human outgrowth endothelial cells leads to IL-8-mediated replicative senescence and impaired vasoreparative function. Stem Cells. 2013;31(8):1657-68.

61. Smadja DM, Bièche I, Uzan G, Bompais H, Muller L, Boisson-Vidal C, et al. PAR-1 activation on human late endothelial progenitor cells enhances angiogenesis in vitro with upregulation of the SDF-1/CXCR4 system. Arterioscler Thromb Vasc Biol. 2005;25(11):2321-7.

62. Bompais H, Chagraoui J, Canron X, Crisan M, Liu XH, Anjo A, et al. Human endothelial cells derived from circulating progenitors display specific functional properties compared with mature vessel wall endothelial cells. Blood. 2004;103(7):2577-84.

63. Smadja DM, Melero-Martin JM, Eikenboom J, Bowman M, Sabatier F, Randi AM. Standardization of methods to quantify and culture endothelial colony-forming cells derived from peripheral blood. Journal of Thrombosis and Haemostasis. 2019;17(7):1190-4.

64. Blandinières A, Randi AM, Paschalaki KE, Guerin CL, Melero-Martin JM, Smadja DM. Results of an international survey about methods used to isolate human endothelial colony-forming cells: guidance from the SSC on Vascular Biology of the ISTH. J Thromb Haemost. 2023;21(9):2611-9.

65. Smadja DM, Melero-Martin JM, Eikenboom J, Bowman M, Sabatier F, Randi AM. Standardization of methods to quantify and culture endothelial colony-forming cells derived from peripheral blood: Position paper from the International Society on Thrombosis and Haemostasis SSC. J Thromb Haemost. 2019;17(7):1190-4.

3

Supplemental Table 1. Antibodies used in immunofluorescence (IF)

Antibody	Manufacturer	Cat. Number	Dilution
IF Primary (OP)			
VWF (rabbit)	DAKO	A0082	1:1000/ 1:50000
VE-cadherin (mouse)	BD Pharming	55561	1:250
β-catenin (rabbit)	Santa Cruz	Sc-7199	1:500
EEA1 (mouse)	BD Biosciences	610457	1:500
Hoechst	Sigma-Aldrich	H3569	1:10000
DAPI	Thermo Fisher	D3571	1:33000
VE-cadherin (goat)	R&D systems	AF938	1:250
VE-cadherin (mouse)	Santa Cruz	sc-9989	1:250
TGN46 (sheep)	Serotec	AHP500	1:1000
IF Primary (OCP)			
VWF (sheep)	Abcam	ab11713	1:1000
VE-cadherin (mouse)	BD Pharming	55561	1:250
Hoechst	Sigma-Aldrich	H3569	1:10000
Rab27A (rabbit)	Protein Tech	17817	1:100
PDI (rabbit)	Enzo Life Sciences	SPA-890	1:250
IF Secondary			
Donkey-anti-Rabbit AF647	Invitrogen Molecular Probes	A31573	1:750
Donkey-anti-Mouse AF568	Invitrogen Molecular Probes	A10037	1:750
Donkey-anti-Sheep AF488	Invitrogen Molecular Probes	A11015	1:750
Donkey-anti Rabbit AF568	Invitrogen Molecular Probes	A10042	1:400
Donkey-anti Goat AF647	Invitrogen Molecular Probes	A32849	1:400
Donkey-anti Mouse CF568	Biotium	20105	1:1000
Donkey-anti Mouse CF488A	Biotium	20014	1:1000

3